Chinese Journal of Aeronautics, (2014),27(6): 1605–1611

Chinese Society of Aeronautics and Astronautics
& Beihang University

Chinese Journal of Aeronautics

cja@buaa.edu.cn
www.sciencedirect.com

A seventh-order model for dynamic response of an electro-hydraulic servo valve

Liu Changhai *, **Jiang Hongzhou**

Department of Fluid Control and Automation, Harbin Institute of Technology, Harbin 150001, China

Received 3 January 2014; revised 17 February 2014; accepted 14 March 2014
Available online 22 October 2014

KEYWORDS

Hydraulic control systems;
Nozzle–flapper;
Servo valve;
Torque motor;
Transfer function

Abstract In this paper, taking two degrees of freedom on the armature–flapper assembly into account, a seventh-order model is deduced and proposed for the dynamic response of a two-stage electro-hydraulic servo valve from nonlinear equations. These deductions are based on fundamental laws of electromagnetism, fluid, and general mechanics. The coefficients of the proposed seventh-order model are derived in terms of servo valve physical parameters and fluid properties explicitly. For validating the results of the proposed model, an AMESim simulation model based on physical laws and the existing low-order models validated by other researchers through experiments are used to compare with the seventh-order model. The results show that the seventh-order model can reflect the physical behavior of the servo valve more explicitly than the existing low-order models and it could provide guidance more easily for a linear control design approach and sensitivity analysis than the AMESim simulation model.

1. Introduction

Two-stage electro-hydraulic servo valves are playing a significant role in high-precision electro-hydraulic servo-systems in which accurate position control is required and have a significant influence on the performance of the whole electro-hydraulic servo-systems. They are capable of converting low electrical signals for precise movements of spools to control high-power on low-speed hydraulic actuators.[1,2]

Many attempts for modeling and studying the dynamic characteristics of electro-hydraulic servo valves and their components have been carried out. For this research area, Merritt[1] has done a lot of useful work to explain the working principle of electro-hydraulic servo valves and proposed an ideal mathematical model for electro-hydraulic servo valves which has been widely distributed and followed by many authors of books and research papers. In later studies, considering the effects of some non-linearities in the form of transfer functions or state-space equations, many other researchers[3,4] established higher-order models which gave a more realistic explanation of the behavior of servo valves. Gordic et al.[5,6] investigated the effects of the variations of torque motor parameters on servo valve performance and also proposed a comprehensive mathematical model of spool position feedback servo valves.

* Corresponding author. Tel.: +86 451 86418318.
E-mail addresses: 13B908002@hit.edu.cn (C. Liu), jianghz@hit.edu.cn (H. Jiang).

Peer review under responsibility of Editorial Committee of CJA.

Production and hosting by Elsevier

http://dx.doi.org/10.1016/j.cja.2014.10.029

Focusing on the performance of a servo valve torque motor, Li et al.[7–9] studied the influence of magnetic fluids on the dynamic characteristics of the torque motor and observed that magnetic fluids could increase the stability of the torque motor. Urata[10–14] has done much useful and significant research on the effects of unequal air gap, magnetic reluctance and leakage flux of permanent magnets, and magnetic stiffness of torque motors. In recent years, Dasgupta and Murrenhoff[15] gave a comprehensive model of a closed-loop servo valve-controlled hydromotor drive system by using the bondgraph simulation technique. Mu and Li[16] deduced a non-linear model to improve the dynamic response of the main spool. Jiao et al.[17,18] investigated the model and matching design of electro-hydraulic load simulator control by a closed-loop servo valve. The cavitation phenomenon in the flapper-nozzle pilot stage of an electro-hydraulic servo valve with an innovative flapper shape was understood in the research of Li et al.[19,20]

However, in previous research, all have supposed an armature–flapper assembly with one degree of freedom. Merritt[1] proposed a third-order model and Kim[3,4] proposed a fifth-order model. The difference between Merritt's model and Kim's model is that the spool valve resonance and pressure feedback on the flapper are ignored in Merritt's model.

In this work, considering an armature–flapper assembly with two degrees of freedom, i.e., a rotation degree provided by electromagnetic torque and a translation degree provided by flow force, a new mathematical model for the dynamic response of two-stage electro-hydraulic servo valves is deduced. State equations are used during the deduction. While the nature of electro-hydraulic servo-systems is nonlinear, it is often desirable to have a linear model for a linear control design approach and sensitivity analysis. Therefore, an accurate linear model for electro-hydraulic servo-systems would be useful for valve design in tailoring the valve dynamics from a control standpoint as well as for high-performance control system design. This new mathematical model offers a seventh-order linear model for the dynamic response of two-stage electro-hydraulic servo valves. At the end of this paper, in order to verify the proposed seventh-order model, an AMESim simulation model based on physical laws and the existing low-order models validated by other researchers through experiments are used to compare with this seventh-order model. The results demonstrate that the seventh-order model can reflect the physical behavior of a servo valve more explicitly than the existing low-order models and it could provide guidance more easily for a linear control design approach and sensitivity analysis than the AMESim simulation model.

2. Working principle of electro-hydraulic servo valves

The schematic diagram of an electro-hydraulic servo valve is illustrated in Fig. 1. This type of electro-hydraulic servo valve consists of two stages[1,2]: the first stage is a double nozzle–flapper valve which consists of a toque motor, a flapper, two nozzles, and a feedback spring, and the second stage is a precision ground four-way control spool.

The function of the nozzle–flapper valve driven by the torque motor through electrical signals is like a hydraulic amplifier putting out a large hydraulic signal to control the position of the spool. Two variable throttle orifices are formed by the annular area between the nozzles and the flapper when the

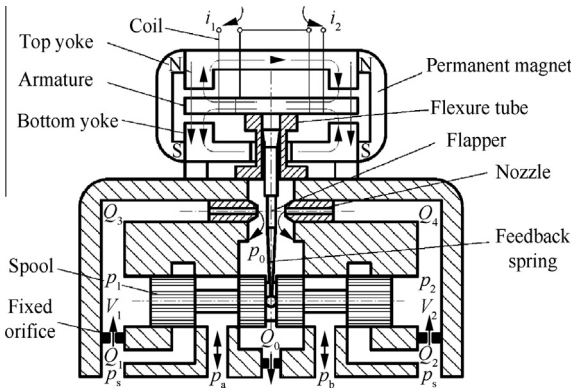

Fig. 1 Schematic diagram of a two-stage electro-hydraulic servo valve.

flapper moves between the two nozzles. Here, i_1 and i_2 are the input electrical signal applied to the coil, p_a and p_b are the inlet or outlet pressure of the load. When there is no electrical signal applied to the coil, the armature stays in the middle between the yokes. This leads the flapper be kept in the middle of the two nozzles, so the pressures at the ends of the spool are equal, and the force balance created by equal pressure in both end chambers holds the spool in a stationary position. When there is an electrical signal applied to the coil, it generates an electromagnetic torque on the armature ends to deflect the armature–flapper assembly from the neutral position. The flapper moves closer to one nozzle decreasing the flow area through this nozzle and letting that of the other nozzle increase. Hydraulic oil is jetted out from both of the nozzles to the flapper, in relation to the two fixed orifices on both sides, which therefore results in a differential pressure over the spool. This differential pressure drives the spool to slide, and the displacement of the spool valve will be fed back to the flapper by the feedback spring. The spool continues to move until the equilibrium between the pressure difference over the spool, the flow forces, and the feedback spring force reaches, and then the servo valve will deliver an output flow proportional to the input current.

3. Mathematical model for dynamic response of servo valve

Fig. 2 shows the schematic diagram of the armature–flapper assembly. Considering the flow force working on the flapper,

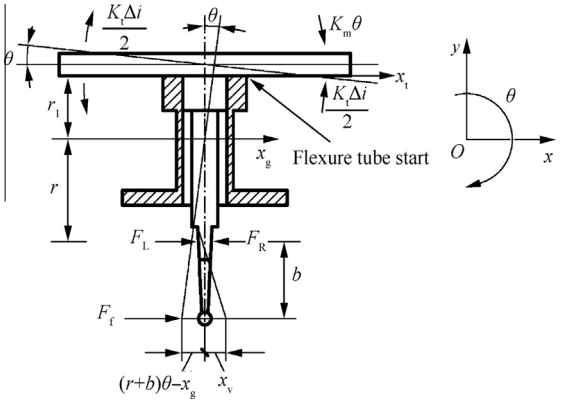

Fig. 2 Schematic diagram of the armature–flapper assembly.

it is assumed in this paper that it has two degrees of freedom, which are the rotational displacement of the armature–flapper assembly and the translational displacement of its center of gravity.[21] The applied torque on the armature results in deflection of the flapper. A change in the position of the flapper caused by an electrical signal creates a differential pressure at the spool ends. As the spool moves due to the differential pressure generated at the spool ends, a restoring torque is developed on the flapper through the mechanical feedback spring. In addition, the cantilever flexure tube has a rotational stiffness and a translational stiffness. Desirable control strategies in the double nozzle-flapper flow control servo valves are the torque balance and the force balance, which ensure that the flapper returns back to the neutral position and the spool attains the equilibrium position.

3.1. Kinematic analysis of torque motor

The net torque applied on the armature–flapper assembly owing to an input differential electrical signal is given by

$$T_{\mathrm{d}} = K_{\mathrm{t}}\Delta i + K_{\mathrm{m}}\theta \tag{1}$$

where T_{d} is the torque produced by the torque motor, K_{t} is the electromagnetic torque constant of the torque motor, K_{m} is the magnetic spring stiffness of the torque motor, Δi is the differential electrical signal applied to the coils, and θ is the angular displacement of the armature.

As shown in Fig. 2, the displacement of the cantilever flexure tube start x_{t} can be described as:

$$x_{\mathrm{t}} = x_{\mathrm{g}} + r_1\theta \tag{2}$$

where x_{t} is the displacement of the flexure tube start, x_{g} is the translational displacement of the armature–flapper assembly's center of gravity, and r_1 is the distance between the center of gravity of the armature–flapper assembly and the flexure tube start.

With the moving of the flapper, the differential pressure on both sides of the nozzles drives the spool to slide a displacement of x_{v}, and thus the fictitious displacement of the spool x_{vf} and the displacement of the flapper x_{f} can be given by:

$$x_{\mathrm{vf}} = x_{\mathrm{g}} - (r+b)\theta \tag{3}$$

$$x_{\mathrm{f}} = x_{\mathrm{g}} - r\theta \tag{4}$$

where r is the distance between the center of gravity of the armature–flapper assembly and the nozzles, and b is the distance between the central line of the nozzles and the central line of the spool.

Based on the material mechanics, the cantilever flexure tube spring stiffness can be acquired by using the following equations:

$$\begin{cases} k_{11} = EI/(L^3/12) \\ k_{12} = k_{21} = EI/(-L^2/6) \\ k_{22} = EI/(L/4) \end{cases} \tag{5}$$

where k_{11}, k_{12}, k_{21}, and k_{22} are the stiffness coefficients of the cantilever flexure tube, E is the Young's modulus for the cantilever flexure tube, I is the moment of inertia of the cantilever flexure tube, and L is the length of the cantilever flexure tube.

According to multi-degree-of-freedom dynamics theory and material mechanics, the force and torque produced by the cantilever flexure tube owing to its deflection can be described as:

$$\begin{bmatrix} F_{\mathrm{tube}} \\ T_{\mathrm{tube}} \end{bmatrix} = \begin{bmatrix} k_{11} & k_{12} \\ k_{21} & k_{22} \end{bmatrix} \begin{bmatrix} x_{\mathrm{t}} \\ \theta \end{bmatrix} \tag{6}$$

where F_{tube} is the force produced by the cantilever flexure tube and T_{tube} is the torque produced by the cantilever flexure tube.

A sketch of the single nozzle–flapper valve is shown in Fig. 3. Here, p_1 is the nozzle inlet pressure and p_0 is the discharged pressure. The pressure distribution on the flapper from p_1 to p_0 is a logarithmic relationship. When the distance between the nozzle and the flapper is small compared with the diameter of the nozzle, this logarithmic relationship can be simplified as a linear relationship.[22]

It has been stated that the significant force on the flapper is resulted from the static pressure acting on the nozzle area projected onto the flapper. The dynamic pressure also acts on the nozzle area projected onto the flapper, and it is of interest to include this effect. Hence, the region occupied by the fluid is divided into three parts. The first part of these regions is subject to pressure p_1 acting on the nozzle area, the second part is subject to a linear gradient pressure between pressure p_1 and pressure p_0 acting on one flapper area, and the third part is subject to pressure p_0 acting on the remaining flapper area. Therefore, the flow force through the left nozzle acting on the flapper can be expressed as

$$\begin{aligned} F_{\mathrm{L}} = {} & p_1\frac{\pi}{4}D_{\mathrm{N}}^2 + p_0\frac{\pi}{4}(D_{\mathrm{f}}^2 - D_{\mathrm{N}}^2) \\ & + \pi\int_{\frac{D_{\mathrm{N}}}{2}}^{\frac{D_{\mathrm{force}}}{2}} \left[p_1 + \frac{p_0 - p_1}{D_{\mathrm{force}} - D_{\mathrm{N}}}(D - D_{\mathrm{N}})\right]\frac{D}{2}\mathrm{d}D \end{aligned} \tag{7}$$

where F_{L} is the flow force through the left nozzle acting on the flapper, p_1 is the pressures on the left side of the spool, D_{N} is the internal diameter of the nozzle, D_{force} is the pressure divisional diameter, p_0 is the discharged pressure, and D_{f} is the diameter of the flapper.

When the flow through the variable throttle orifice is laminar, at this time $D_{\mathrm{force}} = D_{\mathrm{f}}$, and Eq. (7) can be changed as:

$$\begin{aligned} F_{\mathrm{L}} = {} & p_1\frac{\pi}{4}D_{\mathrm{N}}^2 + \frac{\pi}{12}(D_{\mathrm{f}} - D_{\mathrm{N}}) \\ & \times [D_{\mathrm{f}}(2p_0 + p_1) + D_{\mathrm{N}}(p_0 + 2p_1)] \end{aligned} \tag{8}$$

When the flow through the variable throttle orifice is turbulent, at this time $D_{\mathrm{force}} = D_{\mathrm{N}}$, and Eq. (7) can be changed as:

$$F_{\mathrm{L}} = p_1\frac{\pi}{4}D_{\mathrm{N}}^2 + p_0\frac{\pi}{4}(D_{\mathrm{f}}^2 - D_{\mathrm{N}}^2) \tag{9}$$

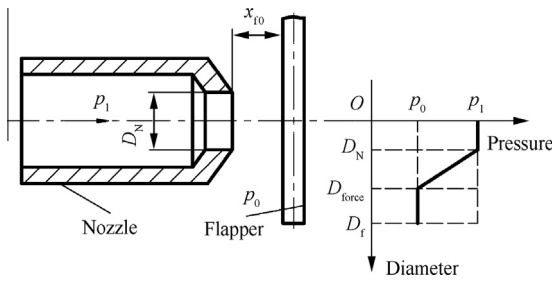

Fig. 3 Sketch of the single nozzle-flapper valve.

Similarly, the flow force through the right nozzle can also be obtained, and thus the net flow force acting on the flapper can be written as:

$$F_{\text{nozzle}} = F_{\text{L}} - F_{\text{R}} \tag{10}$$

where F_{R} is the flow force through the right nozzle acting on the flapper.

The actual displacement of the feedback spring at its end is $x_{\text{g}} - (r + b)\theta - x^{\text{v}}$, and thus the force produced by the feedback spring can be described as:

$$F_{\text{f}} = K_{\text{f}}[(r+b)\theta - x_{\text{g}} + x_{\text{v}}] \tag{11}$$

where F_{f} is the force produced by the feedback spring and k_{f} is the stiffness of the feedback spring.

Apply Newton's second law and multi-degree rigid-body kinetics to the armature–flapper assembly. Equilibrium equations of torque and force on the armature–flapper assembly can be given by

$$\begin{cases} T_{\text{d}} = J\dfrac{\text{d}^2\theta}{\text{d}t^2} + B_{\text{r}}\dfrac{\text{d}\theta}{\text{d}t} + T_{\text{tube}} + F_{\text{f}}(r+b) + T_{\text{nozzle}} \\ F_{\text{nozzle}} + F_{\text{f}} = m\dfrac{\text{d}^2x_{\text{g}}}{\text{d}t^2} + B_{\text{t}}\dfrac{\text{d}x_{\text{g}}}{\text{d}t} + F_{\text{tube}} \end{cases} \tag{12}$$

where J is the moment of inertia of the armature–flapper assembly, B_{r} is the damping coefficient for rotation of the armature–flapper assembly, T_{nozzle} is the torque produced by the net flow force, m is the mass of the armature–flapper assembly, and B_{t} is the damping coefficient for translation of the armature–flapper assembly.

Changing the form of Eq. (12), the torque-motor stage dynamics can be written as a state-space equation:

$$\begin{bmatrix} \dot{\theta} \\ \dot{\omega} \\ \dot{x}_{\text{g}} \\ \dot{v}_{\text{g}} \end{bmatrix} = \begin{bmatrix} 0 & 1 & 0 & 0 \\ \frac{-(K_{\text{f}}(r+b)^2 + k_{21}r_1 + k_{22} - K_{\text{m}})}{J} & \frac{-B_{\text{r}}}{J} & \frac{-(k_{21} - K_{\text{f}}(r+b))}{J} & 0 \\ 0 & 0 & 0 & 1 \\ \frac{(K_{\text{f}}(r+b) - k_{12} - k_{11}r_1)}{m} & 0 & \frac{-(K_{\text{f}} + k_{11})}{m} & \frac{-B_{\text{t}}}{m} \end{bmatrix} \begin{bmatrix} \theta \\ \omega \\ x_{\text{g}} \\ v_{\text{g}} \end{bmatrix} + \begin{bmatrix} 0 & 0 & 0 \\ \frac{K_{\text{t}}}{J} & \frac{-K_{\text{f}}(r+b)}{J} & \frac{-\pi D_{\text{N}}^2 r}{4J} \\ 0 & 0 & 0 \\ 0 & \frac{K_{\text{f}}}{m} & \frac{\pi D_{\text{N}}^2}{4m} \end{bmatrix} \begin{bmatrix} \Delta i \\ x_{\text{v}} \\ p_{\text{Lp}} \end{bmatrix} \tag{13}$$

where $\omega = \frac{\text{d}\theta}{\text{d}t}$, $v_{\text{g}} = \frac{\text{d}x_{\text{g}}}{\text{d}t}$, $p_{\text{Lp}} = p_1 - p_2$, and p_2 is the pressure on the right side of the spool.

3.2. Mathematical model of double nozzle-flapper valve

When the flapper deflects a displacement $x_{\text{g}} - r\theta$ from the neutral position, the flows through the nozzles at both sides are given by the following equations:

$$Q_3 = C_{\text{df}}\pi D_{\text{N}}[x_{\text{f0}} - (r\theta - x_{\text{g}})]\sqrt{\frac{2}{\rho}(p_1 - p_0)} \tag{14}$$

$$Q_4 = C_{\text{df}}\pi D_{\text{N}}[x_{\text{f0}} + (r\theta - x_{\text{g}})]\sqrt{\frac{2}{\rho}(p_2 - p_0)} \tag{15}$$

where Q_3 and Q_4 are the flows through left and right variable throttle orifices, respectively. C_{df} is the flow coefficient of the variable orifice, x_{f0} is the distance between the nozzle and the flapper when the flapper is at the middle place, and ρ is the density of hydraulic oil.

In addition, the flows through the first fixed orifice at both ends are described as follows:

$$Q_1 = C_{\text{d1}}A_1\sqrt{\frac{2}{\rho}(p_{\text{s}} - p_1)} \tag{16}$$

$$Q_2 = C_{\text{d1}}A_1\sqrt{\frac{2}{\rho}(p_{\text{s}} - p_2)} \tag{17}$$

where Q_1 and Q_2 are the flows through the first orifice at both ends, C_{d1} is the flow coefficient of the first fixed orifice, A_1 is the area of the first fixed orifice, and p_{s} is the supply pressure.

The flows Q_3 and Q_4 through the second fixed orifice get together, and the total flow Q_0 goes back to the return pipe whose pressure is nearly atmospheric pressure. Thus the total flow Q_0 can be expressed as:

$$Q_0 = C_{\text{d0}}A_0\sqrt{\frac{2}{\rho}p_0} \tag{18}$$

where Q_0 is the flow through the second orifice, C_{d0} is the flow coefficient of the second fixed orifice, and A_0 is the area of the second fixed orifice.

The fluid compressibility effect at either end of the spool and the leakage flow are considered, and according to the flow continuity theory, the nozzle–flapper stage dynamics are given by

$$\begin{cases} \dot{p}_1 = \frac{\beta_{\text{e}}}{V_1}[Q_1 - Q_3 - A_{\text{v}}v_{\text{v}} - K_{\text{L}}(p_1 - p_2)] \\ \dot{p}_2 = \frac{\beta_{\text{e}}}{V_2}[Q_2 - Q_4 + A_{\text{v}}v_{\text{v}} + K_{\text{L}}(p_1 - p_2)] \end{cases} \tag{19}$$

where β_{e} is the compressibility of hydraulic oil, V_1 and V_2 are the enclosed volumes on each side of the spool, A_{v} is the area of the spool, v_{v} is the speed of the spool, and K_{L} is the coefficient of the leakage flow.

When there is no electrical signal, the armature–flapper assembly and the spool are at their null positions, i.e., $x_{\text{g}} = 0$ and $\theta = 0$. The relationship among these flows can be described as:

$$Q_1 = Q_3 = Q_2 = Q_4 = \frac{1}{2}Q_0 \tag{20}$$

According to Eqs. (14)–(18) and (20), p_1, p_2, and p_0 can be obtained

$$\begin{cases} p_{1\text{e}} = p_{2\text{e}} = \frac{1}{e+1}p_{\text{s}} \\ p_{0\text{e}} = \frac{4f}{e+1}p_{\text{s}} \end{cases} \tag{21}$$

where $e = \frac{(C_{\text{d0}}A_0C_{\text{df}}\pi D_{\text{N}}x_{\text{f0}})^2}{[(C_{\text{d0}}A_0)^2 + 4(C_{\text{df}}\pi D_{\text{N}}x_{\text{f0}})^2](C_{\text{d1}}A_1)^2}$ and $f = \frac{(C_{\text{df}}\pi D_{\text{N}}x_{\text{f0}})^2}{[(C_{\text{d0}}A_0)^2 + 4(C_{\text{df}}\pi D_{\text{N}}x_{\text{f0}})^2]}$. At this time, Eqs. (14)–(17) are linearized at null positions, and substituting these linearized equations into Eq. (19) yields

$$\begin{cases} \dot{p}_1 = \frac{\beta_{\text{e}}}{V_0}[K_{\text{c}}p_1 - K_{\text{x}}x_{\text{g}} + K_\theta\theta - A_{\text{v}}v_{\text{v}} - K_{\text{L}}(p_1 - p_2)] \\ \dot{p}_2 = \frac{\beta_{\text{e}}}{V_0}[K_{\text{c}}p_2 + K_{\text{x}}x_{\text{g}} - K_\theta\theta + A_{\text{v}}v_{\text{v}} + K_{\text{L}}(p_1 - p_2)] \end{cases} \tag{22}$$

where $K_{\text{x}} = C_{\text{df}}\pi D_{\text{N}}\sqrt{\frac{2(p_{1\text{s}} - p_{0\text{e}})}{\rho}}$, $K_\theta = rK_{\text{x}}$, $K_{\text{c}} = -C_{\text{d1}}A_1\sqrt{\frac{1}{2\rho(p_{\text{s}} - p_{1\text{e}})}} - C_{\text{df}}\pi D_{\text{N}}x_{\text{f0}}\sqrt{\frac{1}{2\rho(p_{1\text{s}} - p_{0\text{e}})}}$, and V_0 is the enclosed volume on one side of the spool when the spool is at its neutral place.

Let $p_{\text{Lp}} = p_1 - p_2$, and then equation (22) can be written as

$$\dot{p}_{\text{Lp}} = \frac{\beta_{\text{e}}}{V_0}[(K_{\text{c}} - 2K_{\text{L}})p_{\text{Lp}} - 2K_{\text{x}}x_{\text{g}} + 2K_\theta\theta - 2A_{\text{v}}v_{\text{v}}] \tag{23}$$

3.3. Dynamics analysis of spool

It is found that the servo valve dynamics should not depend on the actuator pressure and the flow rate as they do in the nonlinear model, in order to make the servo valve good for use. The net force on the spool comes from the differential pressure, inertia force, friction force, and the restoring force of the feedback spring. Thus according to Newton's second law, the spool dynamic is given by

$$\begin{bmatrix} \dot{x}_v \\ \dot{v}_v \end{bmatrix} = \begin{bmatrix} 0 & 1 \\ \frac{-K_f}{m_v} & \frac{-B_v}{m_v} \end{bmatrix} \begin{bmatrix} x_v \\ v_v \end{bmatrix} + \begin{bmatrix} 0 & 0 & 0 \\ \frac{A_v}{m_v} & \frac{-K_f(r+b)}{m_v} & \frac{-K_f}{m_v} \end{bmatrix} \begin{bmatrix} p_{Lp} \\ \theta \\ x_g \end{bmatrix} \tag{24}$$

where m_v is the mass of the spool and B_v is the damping coefficient of the spool.

3.4. Transfer function of electro-hydraulic servo valves

Combining Eqs. (13), (23) and (24), the mathematical model of two-stage electro-hydraulic servo valves can be described as a state-space equation:

$$\begin{bmatrix} \dot{\theta} \\ \dot{\omega} \\ \dot{x}_g \\ \dot{v}_g \\ \dot{p}_{Lp} \\ \dot{x}_v \\ \dot{v}_v \end{bmatrix} = \begin{bmatrix} 0 & 1 & 0 & 0 & 0 & 0 & 0 \\ -\frac{K_f(r+b)^2+k_{21}r_1+k_{22}-K_m}{J} & \frac{-B_r}{J} & -\frac{k_{21}-K_f(r+b)}{J} & 0 & -\frac{\pi D_N^2 r}{4J} & -\frac{K_f(r+b)}{J} & 0 \\ 0 & 0 & 0 & 1 & 0 & 0 & 0 \\ \frac{K_f(r+b)-k_{11}r_1-k_{22}}{m} & 0 & -\frac{K_f+k_{11}}{m} & -\frac{B_t}{m} & \frac{\pi D_N^2}{4m} & \frac{K_f}{m} & 0 \\ \frac{2K_0\beta_e}{V_0} & 0 & -\frac{2K_x\beta_e}{V_0} & 0 & \frac{(K_p-2K_L)\beta_e}{V_0} & 0 & -\frac{2A_v\beta_e}{V_0} \\ 0 & 0 & 0 & 0 & 0 & 0 & 1 \\ -\frac{K_f(r+b)}{m_v} & 0 & \frac{K_f}{m_v} & 0 & \frac{A_v}{m_v} & -\frac{K_f}{m_v} & -\frac{B_v}{m_v} \end{bmatrix} \begin{bmatrix} \theta \\ \omega \\ x_g \\ v_g \\ p_{Lp} \\ x_v \\ v_v \end{bmatrix} + \begin{bmatrix} 0 \\ \frac{K_t}{J} \\ 0 \\ 0 \\ 0 \\ 0 \\ 0 \end{bmatrix} \Delta i \tag{25}$$

According to Eq. (25), the transfer function of two-stage electro-hydraulic servo valves can be obtained as

$$\frac{x_v(s)}{\Delta i(s)} = \frac{-b_0 s^3 + b_1 s^2 + b_2 s + b_3}{s^7 + a_1 s^6 + a_2 s^5 + a_3 s^4 + a_4 s^3 + a_5 s^2 + a_6 s + a_7} \tag{26}$$

where a_i and b_i are called model coefficients which are explicitly in terms of the system physical parameters and reveal several model structural properties. These coefficients can be used for sensitivity analysis and design of servo valve dynamics in various ways. If only some parameters of servo valves are known, this proposed model can identify the unknown parameters from experimental data. It can also test the influence on the servo valve dynamics of a given parameter.

It is obvious to know that the derived mathematical model of two-stage electro-hydraulic servo valves is a seventh-order model. This model is different from the models developed by Merritt and Kim. Merritt has derived a third-order model of the following form[1]:

$$\frac{x_v(s)}{\Delta i(s)} = \frac{K_3}{s^3 + h_1 s^2 + h_2 s + h_3} \tag{27}$$

where K_3 and h_i are called model coefficients.

Kim has derived a fifth-order model of the following form[3,4]:

$$\frac{x_v(s)}{\Delta i(s)} = \frac{-n_0 s + n_1}{s^5 + m_1 s^4 + m_2 s^3 + m_3 s^2 + m_4 s + m_5} \tag{28}$$

where n_i and m_i are called model coefficients.

Because it is assumed that the armature–flapper assembly has one degree of freedom in both Merritt's model and Kim's model, besides the spool valve resonance, the pressure feedback on the flapper and the flow forces on the spool are neglected in Merritt's model. Therefore, this new mathematical model assuming the armature–flapper assembly with two degrees of freedom is a supplement to the fifth-order model and the third-order model, which will be validated in the following simulation.

4. Simulation procedure

There is a two-stage electro-hydraulic servo valve simulation model based on physical laws in software AMESim. In order to validate the model derived in this paper, the AMESim simulation model, the fifth-order model derived by Kim, and the third-order model derived by Merritt are used to compare with the seventh-order model derived in this paper. The basic parameters of this two-stage electro-hydraulic servo valve are given in Table 1. The transfer functions of these three mathematical models are given in Appendix A. Fig. 4(a) shows the frequency responses of these three mathematical models and the AMESim simulation model. Fig. 4(b) shows the time step responses of these three mathematical models and the AMESim simulation model when $\Delta i = 1$ mA.

5. Results and discussion

From Fig. 4(a), it can be seen that the seventh-order model fits the AMESim simulation model more closely than the fifth-order model and the third-order model. More specifically, the frequency response of the seventh-order model is almost the same as that of the AMESim simulation model from 10 Hz to 10000 Hz. In contrast, an obvious difference exists between the frequency response of the fifth-order model and that of the AMESim simulation model, although the difference is smaller than that between the third-order model and the AMESim simulation model. Besides, the frequency response of the third-order model starts to deviate from that of the

Table 1 Parameters of the two-stage electro-hydraulic servo valve.

Parameter	Value	Unit
m	0.0055	kg
J	5.8×10^{-7}	kg·m^2
L	4.8	mm
I	0.275	mm^4
E	1.2×10^6	bar
r_1	3	mm
r	8.6	mm
b	13.4	mm
K_f	3400	N/m
K_t	2.1834	N·m/A
K_m	7.9456	N·m/rad
B_t	10	N/(m·s^{-1})
B_r	0.001	N·m/(rad·s^{-1})
x_{f0}	0.06	mm
A_1	0.0314	mm^2
A_0	0.0707	mm^2
V_0	1.1	mm^3
A_v	78.54	mm^2
D_N	0.4	mm
D_f	0.45	mm
ρ	850	kg/m^3
β_e	17,000	bar
m_v	0.01	kg
B_v	50	N/(m·s^{-1})

AMESim simulation model at 10 Hz in the phase plot and there is no resonance peak value in the magnitude plot. In Fig. 4(a), the results show that the magnitudes of the seventh-order model and the AMESim simulation model from 1 Hz to 20 Hz are 29.71 dB; however, those of the fifth-order model and the third model from 1 Hz to 20 Hz are 30.7 dB.

Fig. 4(b) also describes that the seventh-order model renders a better agreement with the AMESim simulation model than the other two models in time step response. It is clear to know that the steady-state values of the seventh-order model and the AMESim simulation model are almost the same with a value of 0.0327 mm. However, the steady-state values of Kim's and Merritt's models are 0.0292 mm, which significantly deviate from that of the AMESim simulation model.

From the frequency and time step responses, the proposed seventh-order model can be validated. The differences between the seventh-order model and the fifth-order model show that the translational displacement of the armature–flapper assembly has an influence on the performance of two-stage electro-hydraulic servo valves, and the differences between the fifth-order model and the third-order model prove the influences of the spool valve resonance and the pressure feedback on the flapper.

In the AMESim simulation model, to reflect physical behaviors of servo valves, a great amount of algorithm needs to be run. Besides, there are some nonlinear terms in the AMESim simulation model. It will take a long time and a great space to finish the simulation. Fortunately, this seventh-order model is a linear mathematical model, so it could provide guidance more easily for a linear control design approach and sensitivity analysis. For instance, if the parameters of servo valves are known, their dynamic characteristics are very clear.

6. Conclusions

The following conclusions can be drawn from this work.

(1) The translational displacement of the center of gravity of the armature–flapper assembly cannot be ignored, which has an influence on the steady-state performance of the servo valve.
(2) This seventh-order model can reflect the physical behavior of the servo valve more precisely than the existing low-order models, and it could provide guidance more easily for a linear control design approach and sensitivity analysis than the AMESim simulation model.

Acknowledgement

The authors would like to give their acknowledgement to the National Natural Science Foundation of China (No. 50975055) for financial support.

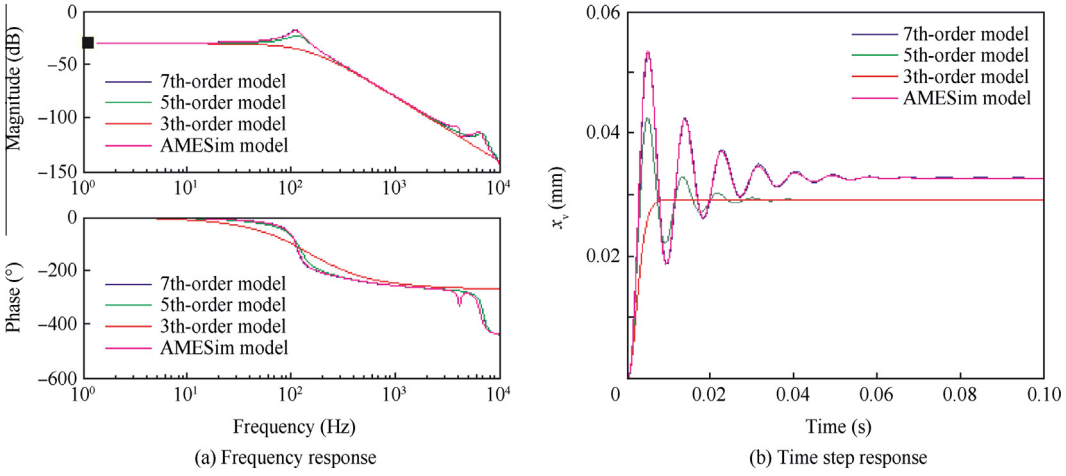

Fig. 4 Frequency and time step responses of the two-stage electro-hydraulic servo valve.

Appendix A.

The seventh-order model:

$$\frac{x_v(s)}{\Delta i(s)} = \frac{-2.8153\times10^{10}s^3 + 4.5725\times10^{16}s^2 + 6.4423\times10^{19}s + 3.1833\times10^{25}}{s^7 + 1.0243\times10^4 s^6 + 2.5856\times10^9 s^5 + 1.2234\times10^{13}s^4 + 1.2466\times10^{18}s^3 + 2.1316\times10^{21}s^2 + 9.5024\times10^{23}s + 9.7211\times10^{26}}$$

The fifth-order model:

$$\frac{x_v(s)}{\Delta i(s)} = \frac{-2.8153\times10^{10}s + 4.5777\times10^{16}}{s^5 + 84246s^4 + 1.9276\times10^9 s^3 + 3.312\times10^{12}s^2 + 1.9215\times10^{15}s + 1.5697\times10^{18}}$$

The third-order model:

$$\frac{x_v(s)}{\Delta i(s)} = \frac{2.3957\times10^7}{s^3 + 2549.9s^2 + 2.4178\times10^6 s + 8.209\times10^8}$$

References

1. Merritt HE. *Hydraulic control systems*. New York: John Wiley and Sons, Inc.; 1967.
2. Li HR. *Hydraulic control systems*. Beijing: National Defense Industry Press; 1990 [Chinese].
3. Kim DH, Tsao TC. An improved linearized model for electro-hydraulic servo valves and its usage for robust performance control system design. *Proceedings of the American control conference*; Albuquerque, New Mexico; 1999. p. 3807–8.
4. Kim DH, Tsao TC. A linearized electro-hydraulic servo valve model for valve dynamics sensitivity analysis and control system design. *ASME J Dynam Syst Meas Control* 2000;**122**(1):179–87.
5. Gordic D, Babic M, Jovicic N, Milovanovic D. Effects of the variation of torque motor parameters on servo valve performance. *J Mech Eng* 2008;**54**(12):866–73.
6. Gordic D, Babic M, Jovicic N, Milovanovic D. Modelling of spool position feedback servo valves. *Int J Fluid Power* 2004;**5**(1):37–51.
7. Li S, Song Y. Dynamic response of a hydraulic servo valve torque motor with magnetic fluids. *Mechatronics* 2007;**17**(8):442–7.
8. Li S, Bao W. Influence of magnetic fluids on the dynamic characteristics of a hydraulic servo valve torque motor. *Mech Syst Signal Process* 2008;**22**(4):1008–15.
9. Li S, Bao W. Influence on dynamic characteristics of a hydraulic servo-valve torque motor due to magnetic fluids. *Chin J Mech Eng* 2008;**44**(12):137–42.
10. Urata E. On the torque generated in a servo valve torque motor using permanent magnets. *Proc IMechE C J Mech Eng Sci* 2007;**221**(5):519–26.
11. Urata E, Shinoda M. Influence of amplifier and feedback on the dynamics of water hydraulic servo valve. *Proceedings of the forth JHPS international symposium on fluid power*; Tokyo, Japan; 1999. p. 567–72.
12. Urata E. Influence of unequal air-gap thickness in servo valve torque motors *Proc IMechE C J Mech Eng Sci* 2007;**221**(11):1287–97.
13. Urata E. Study of magnetic circuits for servo valve torque motors. *Proceeding of Bath workshop on power transmission and control (PTMC)*; Bath, UK; 2000. p. 269–82.
14. Urata E, Suzuki K. Stiffness of the elastic system in a servo valve torque motor *Proc IMechE Part C: J Mech Eng Sci* 2011;**225**(8):1963–72.
15. Dasgupta K, Murrenhoff H. Modelling and dynamics of a servo valve controlled hydraulic motor by bondgraph. *Mech Mach Theory* 2011;**46**(7):1016–35.
16. Mu D, Li C. A new mathematical model of twin flapper-nozzle servo valve based on input–output linearization approach. *Proceedings of 2011 2nd international conference on artificial intelligence management science and electronic commerce (AIMSEC)*; Aug 8–10; 2011. p. 3662–6.
17. Wang C, Jiao Z, Wu S, Shang Y. An experimental study of the dual-loop control of electro-hydraulic load simulator (EHLS). *Chin J Aeronaut* 2013;**26**(6):1586–95.
18. Yao S, Hang Y, Jiao Z, Nan Y. Matching design of hydraulic load simulator with aerocraft actuator. *Chin J Aeronaut* 2013;**26**(2):470–80.
19. Li S, Aung NZ, Zhang S, et al. Experimental and numerical investigation of cavitation phenomenon in flapper–nozzle pilot stage of an electro-hydraulic servo valve. *Comput Fluids* 2013;**88**:590–8.
20. Aung NZ, Li S. A numerical study of cavitation phenomenon in a flapper-nozzle pilot stage of an electro-hydraulic servo valve with an innovative flapper shape. *Energ Convers Manage* 2014;**77**:31–9.
21. Edoqs. Nozzle flapper flow control servo valve [Internet]. [cited 2014 Jan 3]; Available from: http://www.keohps.com/imagine/applications /Servovalves.pdf.
22. Jin CM. Hydro mechanics. Beijing: National Defense Industry Press; 1994 [Chinese].

Liu Changhai is currently a Ph.D. candidate in the Department of Fluid Control and Automation at Harbin Institute of Technology in China, where he received his master's degree in 2013. His research interests include electro-hydraulic servo-systems.

Jiang Hongzhou is currently a professor and Ph.D. advisor at Harbin Institute of Technology in China. His main research interests include electro-hydraulic servo-systems and biomimetic robot.